Appl. Phys. B 52, 1–7 (1991)

Applied Physics B Photo-physics and Laser Chemistry

© Springer-Verlag 1991

Output and Picosecond Amplification Characteristics of an Efficient and High-Power Discharge Excimer Laser

Kenzo Miyazaki, Toru Fukatsu*, Ichiro Yamashita, Toshifumi Hasama, Kawakatsu Yamada, and Takuzo Sato*****

Laser Section, Optoelectronics Division, Electrotechnical Laboratory, 1-1-4, Umezono, Tsukuba, Ibaraki 305, Japan

Received 28 July 1990/Accepted 1 September 1990

Abstract. Improvements in output pulse energy and efficiency of a conventional capacitor-transfer-type discharge excimer laser with automatic preionization have been achieved by extending the discharge volume and resulting moderate pumping of the active medium. The discharge laser produces a pulse energy of more than 1 J for XeCl, KrF, and ArF lasers in square beams of about 2×2 cm^2, and the maximum overall efficiency observed is 2.9% for XeCl, 3.2% for KrF and 1.8% for ArF. The laser device has been involved in a picosecond (~ 32 ps) XeCl laser amplification system, and was operated as an amplifier at a repetitive frequency of 10 Hz. Saturation fluence for XeCl laser was measured to be 1.4 mJ/cm^2, and the picosecond pulse energy of ~ 40 mJ was extracted from the amplifier.

PACS: 42.55, 42.60

In the development of discharge-pumped excimer lasers, continuing improvements in output characteristics have been performed by making use of various techniques. An increase in pulse energy has often been accomplished by high-power loading on the laser gas mixture for a pulsed discharge and/or by extending the discharge duration. However, so far as the laser pumping is done by discharge, an increase in the discharge volume is essential to improve the pulse energy because of some limiting value of electrical energy deposited into the discharge. On the other hand, for the purposes of efficiency improvements, importances are the efficient energy transfer from the pumping circuit to the discharge, optimizations of gas mixtures and pumping power. Of these, in respect to laser design for the efficiency improvement, a moderate pumping is essential [1–4]; for example, the most efficient pumping power for XeCl laser is known to be $1 \sim 2$ MW/cm^3, and an optimization of pumping power has been achieved by a novel spiker-sustainer discharge circuit, where overall efficiencies of more than 4% have been reported [2, 5].

* On leave from Ebara Corp., 6-6-7, Ginza, Chuo-ku, Tokyo 104, Japan

** On leave from Mitsubishi Heavy Industries, LTD., 4-6-22, Kan-on shinmachi, Nishi-ku, Hiroshima 733, Japan

*** Present address: Optoelectronic Industry and Technology Development Association, 20th Mori BLDG., 7-4, Nishi-shinbashi 2-chome, Minato-ku, Tokyo 105, Japan

These principles for improvements in the output characteristics can be applied to an automatically preionized (API) discharge excimer laser, which has been employed extensively for commercial excimer laser systems. Our previous works [3, 6] show that the API discharge excimer laser can be operated efficiently by optimizing the energy transfer into discharge and the pumping power. However, intention to the higher output power inevitably requires a higher pumping power which often results in loosing the high efficiency. An increase in the discharge volume may be a way to satisfy simultaneously the high efficiency and the high output power.

On the other hand, there has been much interest in the amplification of ultrashort ultraviolet (UV) pulses in excimer lasers, and a peak power of more than 10^{11} W has been achieved so far and demonstrated it as an attractive radiation source for a variety of applications such as multiphoton ionization, higher-harmonic generation, and extreme UV laser studies [7–12]. In these studies, discharge-pumped XeCl and KrF excimer lasers have been employed extensively as amplifiers for ultrashort (ps $\sim$ fs) UV laser pulses, and then the increase in the discharge volume and/or the discharge cross section is also essential for the efficient pulse amplification. The maximum amplified pulse energy E that can be extracted is approximated by $E \sim E_s g_0 l S$ [13], where the saturation fluence E_s [J/cm^2] is an intrinsic parameter of the gain medium, g_0 is the small signal gain coefficient depending

on the each device and/or its operational conditions and $g_0 = 0.1 \sim 0.2\,\mathrm{cm}^{-1}$ for discharge pumped XeCl and KrF lasers, l and S are the length of the gain medium and the beam cross section, respectively. Therefore, discharge excimer lasers having a large aperture and/or volume have been developed for the purposes of achieving a large value of lS in ultrashort excimer laser pulse amplification systems [14, 15], while high efficiency of the laser device should be important to develop a reliable and compact system.

This paper reports on an efficient and high-power API discharge excimer laser. It has been developed as an amplifier in an ultrashort pulse amplification system that can be repetitively operated at about 10 Hz. We describe the design of laser, the output characteristics of XeCl, KrF, and ArF lasers, and the results of picosecond XeCl laser pulse amplifications.

1. Laser Design and Apparatus

Figure 1 shows a cross-sectional view (a) and the equivalent electrical circuit (b) of the capacitor-transfer-type API discharge excimer laser constructed, which is of the same type as that previously constructed (hereafter referred to as Laser I) to study efficient operation of discharge-pumped rare-gas halide lasers [3]. The laser was designed to obtain a pulse energy of more than 1 J with XeCl, KrF, and ArF laser oscillators, without loosing the high efficiency achieved in Laser I.

The laser has the total primary (storage) capacitance $C_1 = 120\,\mathrm{nF}$, while the total secondary (discharge) capacitance of $C_2 = 86.4$ or $109.8\,\mathrm{nF}$ is used to see the effects of C_2 on the output characteristics. The laser chamber having two plane-parallel CaF_2 windows of 1.2 cm in thickness is made of nickel-coated aluminum, and the chamber wall is 2.5 cm in thickness. The external dimensions of the chamber are $23.5 \times 39 \times 120\,\mathrm{cm}^3$, including the continuous-gas-circulation system for repetitive operation. The optical resonators for ArF, KrF, and XeCl lasers consisted of one of the CaF_2 windows and an external dielectric-coated total reflector. We employed a thyratron switch (EG & G, model HY-3202).

In designing and constructing the laser, we focused our attention on increasing the discharge volume and achieving a moderate pumping of the active medium, in order to get a simultaneous nature of high efficiency and high power. Although a successful increase in the active volume may be performed by an extension of the electrode spacing, the large spacing often requires a high charging voltage for the efficient operation, especially, of ArF lasers. Moreover, since the laser thresholds of XeCl, KrF, and ArF lasers are usually different, the extension of the spacing leads to a large difference among operational conditions for different kind of excimer lasers. Therefore, to increase the active volume in the conventional type of API excimer laser, we employed a special set of electrodes having different widths, 5 cm for the anode and 3 cm for the cathode. It is well known that most of all discharge pumped excimer laser devices having the same electrode width produce a rectangular beam with a width w narrower than the electrode spacing d even if use is made of a set of well-designed uniform-field electrodes such as one proposed by Chang [16]. The electrode widths in the present device were determined empirically for the spacing $d = 2.2\,\mathrm{cm}$. The central parts of both electrode surfaces, 1.5 cm on the anode and 2.6 cm on the cathode, were shaped in a profile ($k_0 = 0.15$) given by Ernst [17]. The different electrode widths were very effective to broaden the discharge width w, which was confirmed by comparing the discharge width observed using a set of electrodes of the same 5 cm width. This is most likely due to an effective increase in the electric field intensity at the anode edge and resulting field uniformity between the electrodes. The uniform electric field intensity distribution between the electrodes was confirmed by a computer simulation. The nickel-coated solid aluminum electrodes are 100 cm in length and provided an effective discharge length l of 94 cm.

For preionization sparks, an array of 48-nickel-pin gaps is located 3.5 cm apart from the center of electrodes, on both sides of the electrodes. In this configuration, the maximum active volume observed at a charging voltage $V = 36\,\mathrm{kV}$ for C_1 was $d \times w \times l = 2.2 \times 2.2 \times 94\,\mathrm{cm}^3$ for XeCl and KrF lasers, and $2.2 \times 2.0 \times 94\,\mathrm{cm}^3$ for ArF laser. At lower charging voltages of C_1, the discharge width w tended to decrease a little.

The laser has also been designed carefully to achieve a minimum inductance of the discharge circuit. Because the capacitance C_2 used in the present device is rather large,

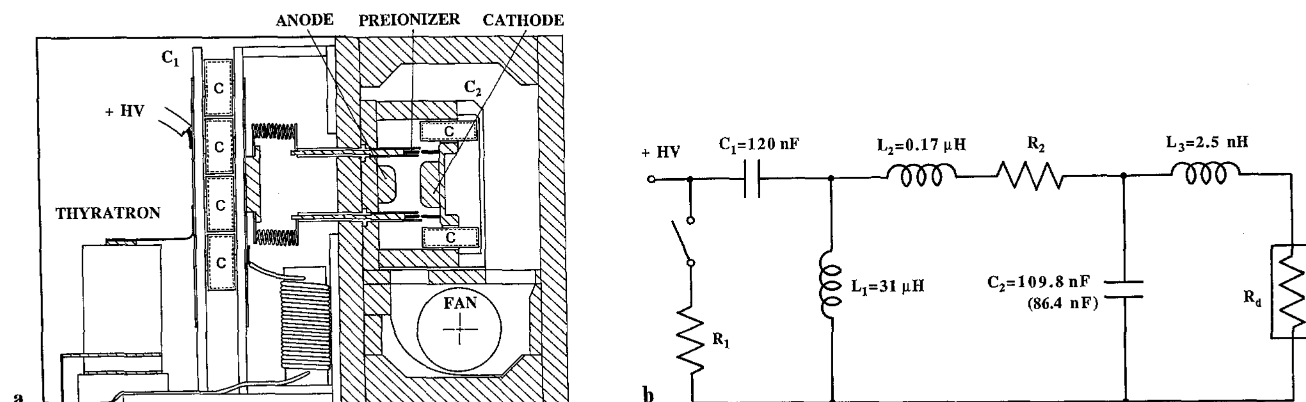

Fig. 1. a Schematic diagram showing a cross sectional view of the API discharge excimer laser. **b** Equivalent electrical circuit of the discharge

the small inductance was essential for efficient power loading resulting from a fast current rise. In the equivalent electrical circuit of the discharge device shown in Fig. 1b, R_1 and R_2 are the resistances of the switch and of the preionization sparks, respectively, L_3 is the circuit inductance for the current flow from C_1 to C_2, and R_d is the resistance of the laser discharge. The circuit parameters were estimated from the temporal changes in the current flow from C_1 to C_2, observed with a Rogowski probe, and in the voltage V_d applied on C_2, with a coaxial high-voltage probe and a $CuSO_4$ resistive divider. The calculated inductance, using the single turn solenoid equation, is 3.3 nH, and is higher than the observed one of 2.5 nH. The smaller value of L_3 observed would originate from the broad discharge width, and provides an expected current rise time, $\sim(L_3C_2)^{1/2}$, of 15 ~ 17 ns.

The high voltage applied on C_2 was observed to rise in a duration $\Delta t = 190 \sim 360$ ns up to a breakdown voltage for the XeCl laser gas mixtures at $V = 17 \sim 36$ kV for a filling gas pressure $P = 6$ atm. The time Δt was larger for the smaller value of V, as discussed in detail in the previous study [3].

The output pulse energy E of XeCl, KrF, and ArF lasers was measured with a Gen-Tec ED-500 joulemeter, while the temporal profile of the laser pulse was observed with a biplanar phototube (Hamamatsu R 1193U-02).

2. Picosecond Pulse Amplification

Experiments were made to study picosecond XeCl pulse amplification characteristics in the laser device constructed. A schematic diagram of the experimental arrangement is shown in Fig. 2. The discharge excimer laser constructed was used as the second amplifier (Amp. II), where the plane-parallel CaF_2 windows were replaced by tilted ones. The amplification system was operated at a repetitive frequency of 10 Hz, and then the Amp. II was operated at a relatively low charging voltage of $V = 22$ kV to suppress the gain and resulting amplified spontaneous emission (ASE) from the long gain medium of $l = 94$ cm. At the same time, the electrode spacing for the discharge was narrowed down to 2.0 cm so as to obtain a square discharge cross section at the low operational voltage.

The picosecond seed pulses are produced by a commercial mode-locked dye laser system (Lumonics, model SPDL) which is synchronously pumped by a (frequency-doubled) mode-locked, Q-switched, pulsed Nd:YAG laser. The dye-laser oscillator and amplifier system is basically the same as described by Hanna et al. [18] and could be operated with a jitter of ± 0.3 ns against external Q-switch trigger pulses for the mode-locked Nd:YAG laser. A single pulse from the Rhodamine 640 dye laser is frequency doubled in a BBO crystal [19], and the UV output is tuned to the gain peak of XeCl laser. The UV radiation with a pulse energy of about 40 μJ is separated with a Pellin-Bloca prism from the visible one and spatially filtered with a 0.1 mm diameter aperture.

The first amplification is made by a commercial excimer laser (Amp. I: Questek, model 2820) with tilted windows. The amplified pulse energy obtained in a beam

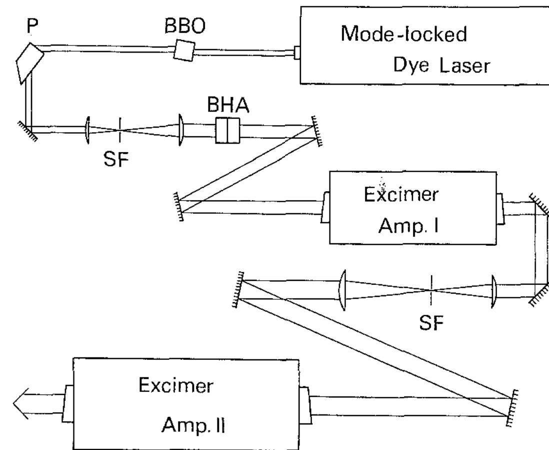

Fig. 2. Experimental arrangement used for the picosecond pulse amplification. Amp. II is the discharge laser device described in the text. (SF: spatial filters; BHA: beam height adjustment)

size of 1×1 cm^2 was about 5 mJ, and this pulse energy was sufficiently large for measurements of amplification characteristics of Amp. II. The amplified spontaneous emission from Amp. I is suppressed with a simple spatial filter consisting of a 50 cm focal length lens and a 0.5 mm diameter aperture. The amplified beam is enlarged to match with the discharge cross section (2×2 cm^2) of Amp. II.

The input and output pulse energies were measured with calibrated Gen-Tec joulemeters (model ED-100A and ED-200), while the temporal shape of a UV pulse was observed with a streak camera (Hamamatsu, model C1587). The typical pulse width (FWHM) was 32 ps. There were some shot-to-shot fluctuations of the widths (20–45 ps) and shapes of the oscillator pulse, and then it was rather difficult to observe the effect of amplification on the modification or stretching of the input pulse. For tuning the UV output wavelength of the oscillator stage and monitoring the amplified spectrum, we employed an optical multichannel analyzer attached on a 1 m grating spectrometer.

The temporal gain widths (FWHM) of Amp. I and Amp. II were about 20 ns, and the timing jitter of amplifiers relative to the trigger pulses was less than ± 2 ns, allowing stable synchronized operations of the oscillator and amplifiers system.

3. Results and Discussion

3.1. Output Characteristics of XeCl, KrF, and ArF Lasers

The output characteristics of the discharge excimer laser constructed were measured in a single pulse operation with XeCl, KrF, and ArF laser gas mixtures at the total pressure $P = 3$–6 atm and $V = 18$–36 kV, where Ne was used as the buffer gas for all kinds of gas mixtures, and the thyratron was replaced by a N_2-filled spark gap switch because of the limited anode voltage and current of the thyratron. The optimization of gas mixtures was made by

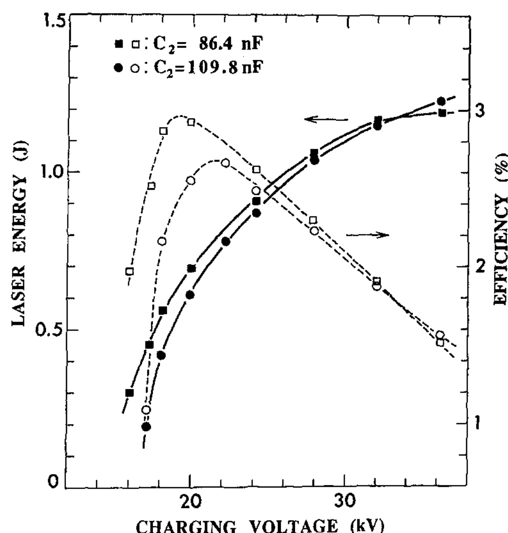

Fig. 3. XeCl laser pulse energy and efficiency as a function of charging voltage for a gas mixture of 4 Torr HCl and 30 Torr Xe in Ne at $P=6$ atm

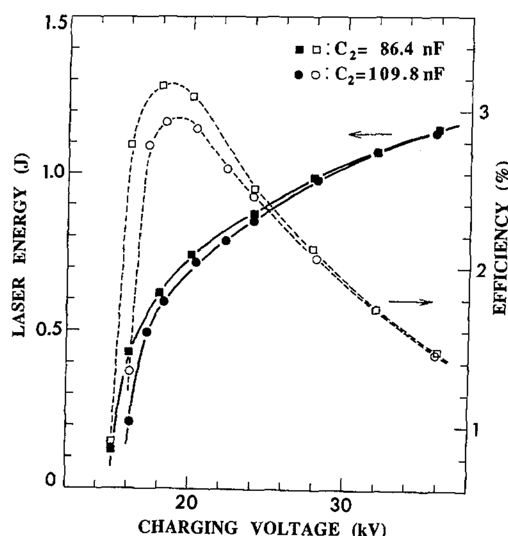

Fig. 5. KrF laser pulse energy and efficiency as a function of charging voltage for a gas mixture of 4 Torr F_2 and 50 Torr Kr in Ne at $P=4$ atm

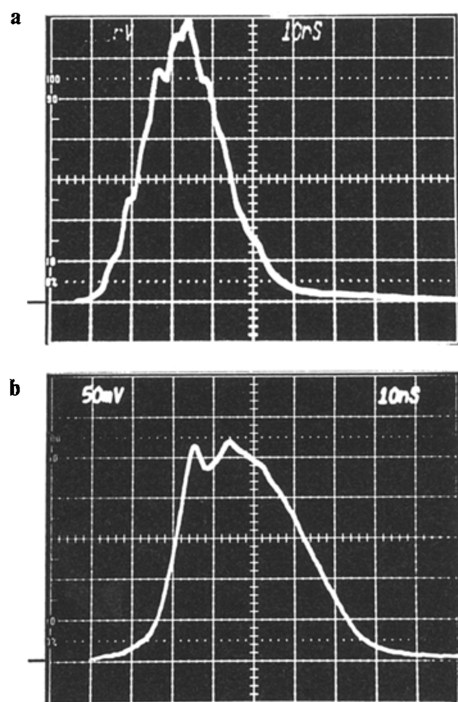

Fig. 4a, b. Temporal change in the XeCl laser emission at $V=36$ kV for **a** $C_2=86.4$ nF and **b** $C_2=109.8$ nF. The gas mixture is the same as in Fig. 3. The time scale is 10 ns/div

referring to those of Laser I, but small differences were observed.

Figure 3 shows the XeCl laser pulse energy E and the overall efficiency η for $C_2=86.4$ nF and 109.8 nF as a function of charging voltage V for a gas mixture of 4 Torr HCl and 30 Torr Xe at $P=6$ atm. The output energy increases monotonically with increasing V, while the overall efficiency η shows a peak value at a relatively low charging voltage. These characteristic changes in E and η are similar to those observed with Laser I and have been discussed in detail in [3]. The pulse energy E of 1.23 J was obtained at $V=36$ kV for $C_2=109.8$ nF, and then the active volume V_g was 455 cm^3, which was estimated from the observed output beam cross section of 2.2×2.2 cm^2 and the discharge length of 94 cm. The maximum energy extraction of 2.6 J/l is less than a half of that (5.8 J/l) obtained with Laser I ($V_g=116$ cm^3, $E=0.68$ J) under nearly the same discharge conditions. This suggests that the pumping power for a unit active volume in the present device is much smaller than that in Laser I, as will be described later. The highest efficiency η observed with XeCl laser is 2.9% with $E=0.70$ J at $V=20$ kV for $C_2=86.4$ nF, as shown in Fig. 3. The 27% increase in C_2 is found to neither lead to an effective improvement in E nor in η.

Figure 4 shows the temporal changes in XeCl laser pulses observed at $V=36$ kV and $P=6$ atm for the two different values of C_2. The laser pulse widths (FWHM) are 22 and 34 ns for $C_2=86.4$ and 109.8 nF, respectively. Although the increase in C_2 decreases the current rise determined by $\sim(L_3C_2)^{1/2}$, one may expect an increases in the peak discharge current that is approximately proportional to $V_b(C_2/L_3)^{1/2}$, and resulting output energy. However, in the XeCl laser the pumping tends to easily saturate due to the relatively low breakdown voltage, as shown later, and/or to the relatively low threshold of lasing, and then only the discharge duration (or laser pulse duration) is observed to lengthen for the larger value of C_2.

The output characteristics measured with KrF laser were similar to those of XeCl laser shown in Fig. 3. Figure 5 depicts E and η measured as a function of V for a gas mixture of 4 Torr F_2 and 50 Torr Kr at $P=4$ atm, where the highest overall efficiency of 3.2% is observed with $E=0.62$ J at $V=18$ kV for $C_2=86.4$ nF. On the other hand, the maximum pulse energy of $E=1.34$ J was obtained with $\eta=1.7$% for a gas mixture of 4 Torr F_2 and 50 Torr Kr at $P=6$ atm and $V=36$ kV for $C_2=109.8$ nF. The increase in C_2 from 86.4 to 109.8 nF improved

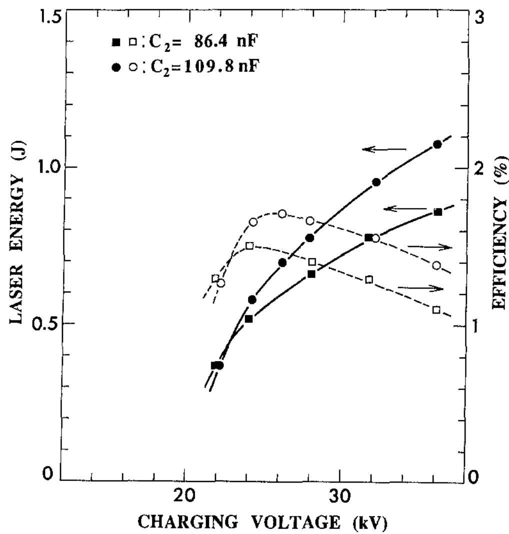

Fig. 6. ArF-laser pulse energy and efficiency as a function of charging voltage for a gas mixture of 3 Torr F_2 and 150 Torr Ar in Ne at $P = 6$ atm

appreciably E of KrF laser only in the region of higher charging voltage ($V > 25$ kV) at $P = 6$ atm. In contrast to those of XeCl laser, the pulse widths observed for the different values of C_2 at $V = 36$ kV and $P = 6$ atm were nearly the same, 31 ns for 86.4 nF and 33 ns for 109.8 nF.

With the increase in C_2, the most significant improvements in E and η were observed with ArF laser, as shown in Fig. 6. The maximum pulse energy of 1.07 J ($\eta = 1.4\%$) was obtained for a gas mixture of 3 Torr F_2 and 150 Torr Ar at $P = 6$ atm, while the highest efficiency observed was 1.8% ($E = 0.52$ J) at $V = 22$ kV for the same gas mixture at $P = 4$ atm. The observed pulse widths were 20 ~ 21 ns, and no appreciable change in the width was observed for the different values of C_2. With the increase in C_2, E was increased by about 25% at $V = 36$ kV for $P = 6$ atm. This effective improvement in E of ArF laser is due to the higher pumping power required for its efficient operation. To our knowledge, the highest ArF laser pulse energy obtained so far with the discharge device is 2 J ($\eta = 0.51\%$), where a very high excitation voltage of about 70 kV has been used for the 3.5 cm electrode spacing at $P = 5$ atm [20]. In spite of the relatively low operational voltage, the efficient pumping in the present device was realized with the fast current rise resulting from the low inductance of discharge circuit.

The output characteristics of three different excimer lasers of interest imply that an optimum design of a discharge pumped excimer laser depends on each kind of gas mixture employed. To see this in more detail, we measured the breakdown voltage V_b in the gas mixtures for XeCl and ArF lasers, and the results at $P = 6$ atm are exhibited in Fig. 7a. The breakdown voltage V_b in the ArF laser is clearly seen to be much higher than that in the XeCl laser. Figure 7b shows the energy transfer rate η_1 from C_1 to C_2, and the electrical efficiency η_2, defined as $\eta_2 = E/(1/2)C_2V_b^2$ and discussed in [3]. The high value of V_b in the ArF leads to η_1 higher than that in the XeCl laser, but η_2 in the ArF is much lower than that in the XeCl.

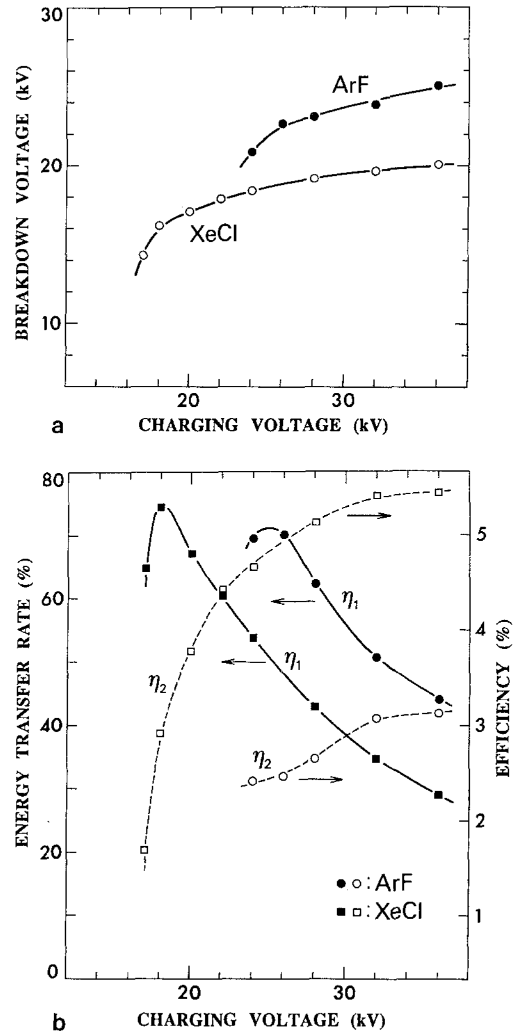

Fig. 7. a Breakdown voltage and **b** the energy transfer rate η_1 and the electrical efficiency η_2 in XeCl and ArF lasers as a function of charging voltage for the same gas mixture as in Figs. 4 and 6

These facts suggest that the ArF laser requires a pumping power much higher than the XeCl, so as to obtain a high output energy of the same level as that of the XeCl and/or the KrF lasers (Fig. 6).

Under the same discharge conditions at $V = 36$ kV as in Fig. 7, we calculated the discharge characteristics in the XeCl and ArF lasers, using the observed temporal change in the voltage V_d applied on C_2 and the circuit parameters shown in Fig. 1b. In the calculation we have assumed an exponential decrease in the discharge resistance R_d as $R_d = R_a + R_b \exp(-t/\tau)$, where $R_a (\ll R_b)$ is the steady state value of the avalanche discharge, R_b is the resistance just before the breakdown at $t = 0$, and τ is the characteristic time of the breakdown or current rise, as described in detail in the previous studies [3, 21]. The calculated temporal changes in V_d, the discharge current I_d or current density i_d, the pumping power P_d or pumping intensity p_d, and the deposition energy E_d into the discharge are shown in Fig. 8a and b for the XeCl and ArF lasers, respectively. The characteristic differences between XeCl and ArF laser discharges are clearly seen, supporting the above discussions: The higher value of V_b in the ArF results in the

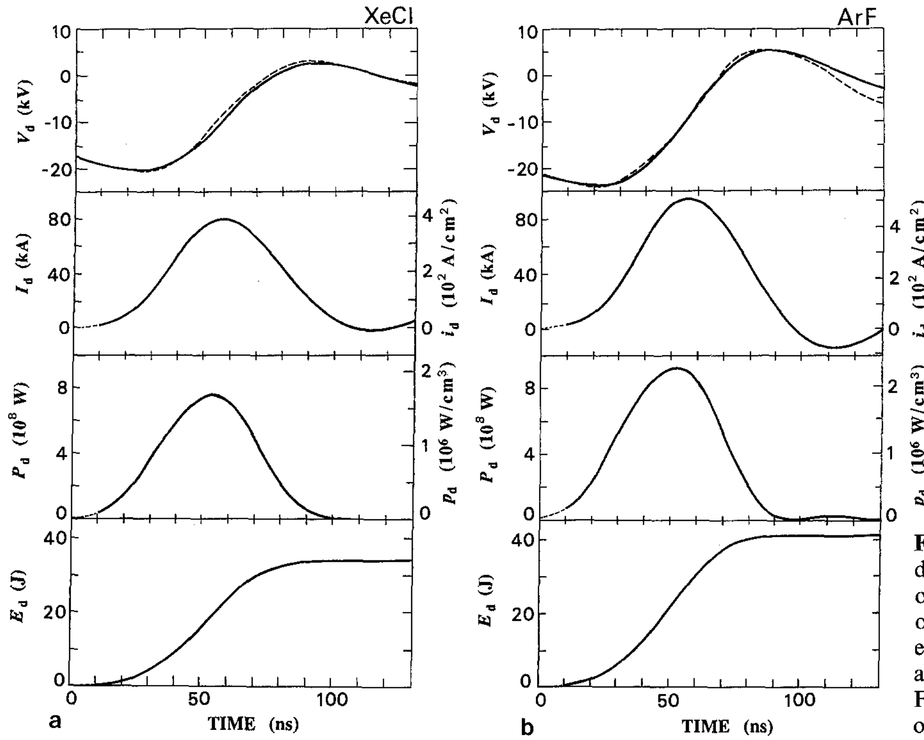

Fig. 8a, b. Calculated temporal changes in the discharge voltage V_d, the discharge current I_d or current density i_d, the pumping power P_d or pumping intensity p_d, and the deposition energy E_d in the **a** XeCl and **b** ArF lasers at $V=36$ kV for the same gas mixtures as in Fig. 7. The dashed curve of V_d is the observed one

higher pumping power and higher deposition energy, while the intrinsic efficiency of ArF is much lower than that of XeCl. We may conclude that in the ArF laser the efficiency lower than that in the XeCl comes from the lower excimer formation efficiency inherent to the ArF laser discharge, and the higher pumping intensity p_d should be used to improve the output energy. The intrinsic efficiency of ArF laser observed, which may be approximated by η_2, is comparable to that ($\sim$4%) calculated and expected by Ohwa and Obara [22].

2.2. Picosecond Pulse Amplification

Figure 9 shows the UV spectra from the oscillator stage and the Amp. II which was observed about 3 m apart from the output window of Amp. II, where the XeCl laser spectrum are shown for comparison. The accurate spectral bandwidth of picosecond pulses was not measured, because the observed one ($\sim$0.05 nm) was comparable with the spectral resolution ($\sim$0.03 nm) of our detection system. Within the detection limit, no appreciable broadening of the spectrum was observed at the amplifier stages.

Measurement of the picosecond XeCl (Amp. II) laser gain was made using the collimated 2×2 cm^2 beam, and the result is shown in Fig. 10. The solid and dashed curves in Fig. 10 are the calculated values according to the usual Franz-Nodvik formula [13]

$$E_{\text{out}}=E_s\ln\{1+\exp(g_0L)[\exp(E_{\text{in}}/E_s)-1]\}, \tag{1}$$

where E_{in} and E_{out} are the input and output fluences [W/cm^2], respectively. Taking into account of uncertainties in the pulse energy measurements, the experimental data give $g_0=0.8\pm0.05$ and $E_s=1.4\pm0.2$ mJ/cm^2.

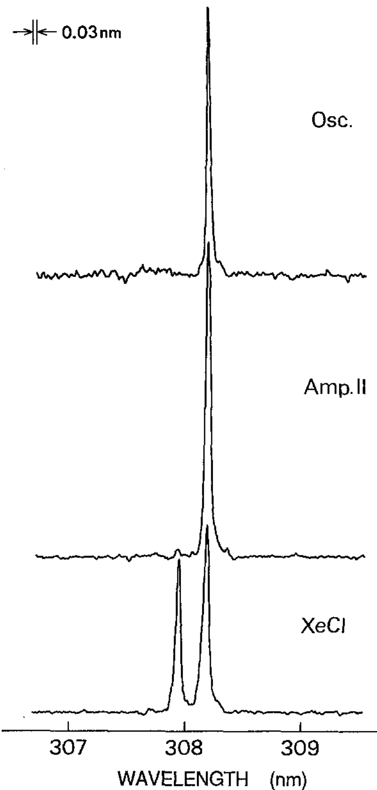

Fig. 9. Output UV spectra from the oscillator stage (upper) and the Amp. II (middle) in the picosecond pulse amplification system. The lower is the XeCl laser emission spectrum for reference

Nearly the same amplification characteristics were observed, when the wavelength of picosecond pulses was tuned to the other gain peak (Fig. 9) of the XeCl laser.

So far, several experimental values of the saturation fluence have been reported on XeCl lasers. Those are in a

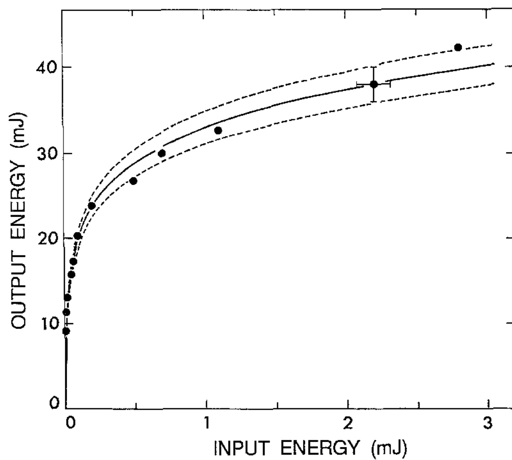

Fig. 10. Picosecond XeCl laser pulse amplification characteristics observed with Amp. II. The laser was operated at a repetition rate of 10 Hz at $V=22$ kV for a gas mixture of 2 Torr HCl and 30 Torr Xe in Ne at $P=4$ atm. The solid curve is the best fit to the Frantz-Nodvik formula with $E_S=1.4\,\mathrm{mJ/cm^2}$ and $g_0=0.08$, and the dashed curves with $E_S=1.5\,\mathrm{mJ/cm^2}$ (upper) and $E_S=1.3\,\mathrm{mJ/cm^2}$ (lower)

range of $E_s=0.85\sim2.5\,\mathrm{mJ/cm^2}$ for XeCl laser pulses of $0.22\sim600$ ps. The present value obtained agrees well with those measured by Corkum and Taylor [23], 1.0–1.2 mJ/cm^2 for 2 ps pulses, and Taylor et al. [24] and Akhmanov et al. [25], 1.0 mJ/cm^2 for $0.16\sim6.0$ ps pulses.

As for the gain dynamics in an XeCl laser amplifier, it has been found that two cases should be distinguished due to the two-component gain recovery with time constants of 40–50 ps and a few ns [23, 26]. Several researchers have concluded that E_s is $\sim2.5\,\mathrm{mJ/cm^2}$ for long input pulses ($>\sim200$ ps), while E_s is $\sim1.0\,\mathrm{mJ/cm^2}$ for short pulses less than 5 ps [23, 24, 26]. Although the detail of XeCl laser gain dynamics appears to be rather complicated, the present result observed may suggest that the fast recovery of gain should influenced on E_s for the pulse width of 30–40 ps.

The relatively low gain coefficient g_0 obtained results from the special design of our laser with the low pumping power, as well as from the low operational voltage. This design for a low pumping power is very effective to suppress the ASE. In fact, despite the long gain medium used, the ASE included in the $2\times2\,\mathrm{cm^2}$ beam was less than 5 mJ, which was measured about 2 m apart from the output window. The weak ASE was tolerable for an application of the laser system to the generation of coherent extreme UV radiation by nonlinear frequency conversion in rare gases, and we have observed the ninth-harmonic generation at 34.2 nm. The results of harmonic generation will be reported elsewhere.

Further experimental investigations should be necessary for complete understandings of the gain dynamics in the XeCl laser amplifier, because the data reported so far seem to be rather scattered. We are now planning a detailed study of the gain dynamics using subpicosecond XeCl laser pulses, as well as further amplification of ultrashort pulses with the X-ray preionized large-aperture discharge excimer laser developed [14].

4. Conclusions

We have developed an efficient and high-power API discharge excimer laser and studied in detail the output characteristics. It has been shown that the increase in the discharge width and resulting discharge volume are very effective to achieve the moderate pumping for high efficiency and to extract the large pulse energy. The pulse energies of more than 1 J for XeCl, KrF, and ArF lasers have been obtained from the conventional type and normal size of discharge device. The laser developed was involved in a picosecond XeCl pulse amplification system, and the amplification characteristics were measured. The saturation fluence measured was 1.4 mJ/cm^2, and the picosecond pulse energy of ~40 mJ has been extracted, providing useful repetitive high-peak-power ($\sim$GW) UV laser pulses.

Acknowledgements. The authors would like to thank K. Ono and K. Kudo for their help in the experiments, and J. Shimada for his encouragement and support.

References

1. R.S. Taylor, P.B. Corkum, S. Watanabe, K.E. Leopold, A.J. Alcock: IEEE J. QE-**19**, 416 (1983)
2. W.H. Long, Jr., M.J. Plummer, E.A. Stappaerts: Appl. Phys. Lett. **43**, 735 (1983)
3. K. Miyazaki, T. Hasama, K. Yamada, T. Fukatsu, T. Eura, T. Sato: J. Appl. Phys. **60**, 2721 (1986)
4. Q. Lou: Opt. Commun. **65**, 26 (1988)
5. C.H. Fisher, M.J. Kushner, T.E. Dehart, J.P. McDaniel, R.A. Petr, J.J. Ewing: Appl. Phys. Lett. **48**, 1574 (1986)
6. K. Miyazaki, Y. Toda, T. Hasama, T. Sato: Rev. Sci. Instrum. **56**, 201 (1985)
7. S. Szatmári, F.P. Schäfer, E. Müller-Horsche, W. Mückenheim: Opt. Commun. **63**, 305 (1987)
8. S. Watanabe, A. Endoh, M. Watanabe, N. Sarukura: Opt. Lett. **13**, 580 (1988)
9. J.R.M. Barr, N.J. Everall, C.J. Hooker, I.N. Ross, M.J. Shaw, W.T. Toner: Opt. Commun. **66**, 127 (1988)
10. A. Endoh, M. Watanabe, N. Sarukura, S. Watanabe: Opt. Lett. **14**, 353 (1989)
11. T.S. Luk, A. McPherson, G. Gibson, K. Boyer, C.K. Rhodes: Opt. Lett. **14**, 1113 (1989)
12. A.J. Taylor, C.R. Tallman, J.P. Roberts, C.S. Lester, T.R. Gosnell, P.H.Y. Lee, G.A. Kyrala: Opt. Lett. **15**, 39 (1990)
13. L.M. Frantz, J.S. Nodvik: J. Appl. Phys. **34**, 2346 (1963)
14. T. Hasama, K. Miyazaki, K. Yamada, T. Sato: IEEE J. QE-**25**, 113 (1989)
15. M. Steyer, K.A. Stankov, H. Mizoguchi, B. Ouyang, F.P. Schäfer: Appl. Phys. B **49**, 331 (1989)
16. T.Y. Chang: Rev. Sci. Instrum. **44**, 405 (1973)
17. G.J. Ernst: Opt. Commun. **49**, 275 (1984)
18. D.C. Hanna, D.J. Pointer, K.A. Ure: IEEE J. QE-**22**, 1117 (1986)
19. K. Miyazaki, H. Sakai, T. Sato: Opt. Lett. **11**, 797 (1986)
20. J.E. Andrew, P.E. Dyer, P.J. Roebuck: Opt. Commun. **49**, 189 (1984)
21. K. Yamada, K. Miyazaki, T. Hasama, T. Sato: Appl. Phys. Lett. **54**, 597 (1989)
22. M. Ohwa, M. Obara: J. Appl. Phys. **63**, 1306 (1988)
23. P.B. Corkum, R.S. Taylor: IEEE J. QE-**18**, 1962 (1982)
24. A.J. Taylor, T.R. Gosnell, J.P. Roberts: Opt. Lett. **15**, 118 (1990)
25. S.A. Akhmanov, V.M. Gordienko, M.S. Dzhidzhoev, S.V. Krayushkin, I.A. Kudinov, V.T. Platonenko, V.P. Popov: Sov. J. Quantum Electron. **16**, 1291 (1987)
26. S. Szatmári, F.P. Schäfer: J. Opt. Soc. Am. B **4**, 1943 (1987)